arXiv:1606.06118v1 [cond-mat.mes-hall] 20 Jun 2016

Strong spin Seebeck effect in Kondo T-shaped double quantum dots

Krzysztof P. Wójcik* and Ireneusz Weymann
Faculty of Physics, Adam Mickiewicz University, Umultowska 85, 61-614 Poznań, Poland
(Dated: June 21, 2016)

We theoretically investigate the thermoelectric and spin thermoelectric properties of a T-shaped double quantum dot strongly coupled to two ferromagnetic leads, focusing on transport regime where the system exhibits the two-stage Kondo effect. We study the dependence of the (spin) Seebeck coefficient, the corresponding power factor and the figure of merit on temperature, leads' spin polarization and dot level position. We show that the thermal conductance fulfills a modified Wiedemann-Franz law. We also demonstrate that the spin thermopower is enhanced at temperatures corresponding to the second stage of Kondo screening. Very interestingly, the spin-thermoelectric response of the system is found to be highly sensitive to the spin polarization of the leads. In some cases spin polarization of the order of 1% is sufficient for a strong spin Seebeck effect to occur. This is explained as a consequence of the interplay between the two-stage Kondo effect and the exchange field induced in the double quantum dot. All calculations are performed with the aid of numerical renormalization group technique.

I. INTRODUCTION

The thermoelectric properties of matter have drawn the attention of physicists since the first experiments carried out by Seebeck at the beginning of the 19th century. While the properties of bulk materials are already quite well understood [1], the problem of thermoelectricity in confined nanoscale systems still contains issues that need further examination, although these have been intensively researched since the famous publications by Hicks and Dresselhaus [2, 3]. In particular, thermoelectric and spin-thermoelectric properties of strongly correlated quantum dot (QD) systems constitute a field of intensive research [4–14]. It turns out that the understanding of thermoelectric transport properties is not only relevant for possible future applications, but also provides additional information about fundamental interactions and phenomena at the nanoscale. One prominent example is undoubtedly the Kondo effect [15], which has been attracting the attention of scientists for more than two decades [16, 17]. In fact, the Seebeck coefficient for the Kondo quantum dots was not only reliably calculated [18], but also measured [19]. Moreover, the thermopower was also analyzed for double quantum dot (DQD) systems in the isospin Kondo regime, in which the device was shown to work as a minimal thermoelectric generator [20].

In the presence of magnetic field or when the leads are ferromagnetic, the thermoelectric response of the system becomes spin polarized [4, 5]. Spin caloritronic effects of single quantum dots in the Kondo regime were already studied theoretically [21–23]. Moreover, although spin-resolved thermoelectricity was also a subject of investigations for DQD systems [24, 25], there are still problems that need further considerations. In particular, in this paper we analyze the spin caloritronic properties of a T-shaped DQD coupled to two ferromagnetic leads in the Kondo regime. The schematic of the considered system is depicted in Fig. 1. Despite its relative simplicity, this system hosts a variety of interesting many-body phenomena. The screening of subsequent quantum dots gives rise to the two-stage Kondo effect, introducing a cryogenic temperature scale T^* associated with the second stage of screening [26, 27, 30]. On the other hand, the dependence of the Kondo temperature T_K and T^* on the DQD level position can lead to Fano-like interference effects [28–32]. It was shown recently that these phenomena are reflected in thermoelectric properties of the device [25]. Here we extend these studies to more complex, magnetic system.

We note that the influence of magnetism on strongly correlated regime of T-shaped DQDs was already discussed, but mainly in the context of electrical properties, such as linear conductance and current spin polarization. The spin-dependent Fano antiresonance condition in magnetic field [33] and in system with ferromagnetic leads [34] was predicted. Moreover, the interplay of the two-stage Kondo screening and the ferromagnets-induced

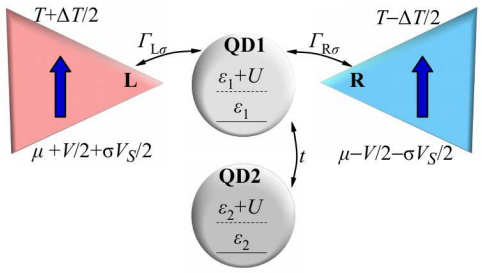

Figure 1. Schematic of the system. The left (L) and right (R) leads are coupled to the main quantum dot (QD1) via spin-dependent couplings $\Gamma_{L\sigma}$ and $\Gamma_{R\sigma}$. The second quantum dot (QD2) is directly coupled only to QD1, with a matrix element t. A small voltage V (correspondingly spin voltage V_S) shifts (spin-splits) otherwise equal chemical potentials $\mu_L = \mu_R = \mu$ symmetrically. There is also a temperature gradient ΔT applied symmetrically to the system.

* kpwojcik@amu.edu.pl

exchange field was also studied [35]. The goal of this paper it to investigate the spin thermoelectric properties of the magnetic device. It is shown that the spin caloritronic coefficients are strongly affected by the presence of ferromagnetic correlations. Spin polarization of the order of 1% can already induce a strong spin Seebeck effect in transport regime where the second stage of screening develops.

We would also like to note that although direct observation of the spin Seebeck effect was already reported [36, 37], in quantum dot systems it still remains a challenge. Therefore, we believe that our results will, on one hand, stimulate further experimental efforts and, on the other hand, be of assistance in understanding future experimental data.

The paper is organized as follows. In Sec. II the model of the device and method used for its solution are explained. The relevant energy scales are outlined in Sec. III. Main results, concerning the calculated Seebeck and spin Seebeck coefficients are presented and discussed in Sec. IV. Finally, Sec. V concludes the paper.

II. MODEL AND METHODS

The considered device consists of two single-level quantum dots in a T-shaped geometry with the first quantum dot (QD1) coupled to external ferromagnetic leads and the second dot (QD2) attached to the first one through the hopping matrix elements t, see Fig. 1. The system can be thus described by the following two-impurity Anderson Hamiltonian [38], $H = H_{\rm DQD} + \sum_r H_r + H_{\rm tun}$. The first term corresponds to isolated DQD and is given by

$$H_{\rm DQD} = \sum_{i\sigma} \varepsilon_i n_{i\sigma} + U \sum_i n_{i\uparrow} n_{i\downarrow} + \sum_\sigma t(d^\dagger_{1\sigma} d_{2\sigma} + h.c.)\,, \tag{1}$$

where $n_{i\sigma} = d^\dagger_{i\sigma} d_{i\sigma}$ and $d^\dagger_{i\sigma}$ creates a spin-σ electron in dot i with the corresponding energy ε_i and U is the Coulomb correlation parameter in each dot. The ferromagnetic leads are modeled by free-electron Hamiltonian $H_r = \sum_{\vec{k}\sigma} \varepsilon_{r\vec{k}\sigma} n_{r\vec{k}\sigma}$ ($r = L$ for left and $r = R$ for right lead, $n_{r\vec{k}\sigma}$ denotes the occupation operator for state characterized by momentum $\vec{k}$, spin σ and lead r, while $\varepsilon_{r\vec{k}\sigma}$ is the energy of the corresponding level). The coupling between the first dot and the leads is described by the tunneling Hamiltonian $H_{\rm tun} = \sum_{r\vec{k}\sigma} v_{\vec{k}\sigma}(d^\dagger_{1\sigma} c_{r\vec{k}\sigma} + h.c.)$, where $c_{r\vec{k}\sigma}$ is the corresponding annihilation operator and $v_{\vec{k}\sigma}$ denotes the respective tunnel matrix element.

We consider the wide-band limit and assume that only s-waves couple to the electrodes. This allows us to write the spin-dependent coupling $\Gamma_{r\sigma} = \pi\rho_{r\sigma}|v_{\vec{k}\sigma}|^2$ as a constant ($\rho_{r\sigma}$ denotes the normalized spin-resolved density of states of lead r at the Fermi level), determined by the leads' spin polarization p_r. For parallel configuration of the magnetizations of the leads, one then gets $\Gamma_{r\sigma} = (1 + \sigma p_r)\Gamma_r/2$, and $\Gamma_\sigma \equiv \Gamma_{L\sigma} + \Gamma_{R\sigma} = (1 + \sigma p)\Gamma$, where $p = (p_L + p_R)/2$ is the effective leads' spin polarization and we assumed $\Gamma_L = \Gamma_R \equiv \Gamma/2$. We note that in the antiparallel magnetic configuration, for left-right symmetric systems, the couplings become spin independent and the transport properties are similar to those in the nonmagnetic case with a polarization dependent factor. On the other hand, when the system is not symmetric, the behavior is the same as in the case of parallel magnetic configuration with some new coupling strength and effective spin polarization [39]. Therefore, in the following we will consider only the case of parallel magnetic configuration.

Let I_x denote the x-current ($x = C$ for charge, $x = S$ for spin, $x = Q$ for heat). Using the Boltzmann equation approach and assuming well-defined Fermi level to be the reference point for energy scale, one can derive the linear-response coefficients connecting currents with voltage V, spin voltage V_S and temperature difference ΔT [1]

$$\begin{pmatrix} I_C \\ I_S \\ I_Q \end{pmatrix} = \sum_\sigma \begin{pmatrix} e^2 L_{0\sigma} & \sigma e^2 L_{0\sigma} & -eL_{1\sigma}/T \\ -\sigma e\frac{\hbar}{2} L_{0\sigma} & -e\frac{\hbar}{2} L_{0\sigma} & \sigma\frac{\hbar}{2} L_{1\sigma}/T \\ -eL_{1\sigma} & -\sigma eL_{1\sigma} & L_{2\sigma}/T \end{pmatrix} \begin{pmatrix} V \\ V_S \\ \Delta T \end{pmatrix}, \tag{2}$$

where e is the absolute value of electron charge,

$$L_{n\sigma} = -\frac{1}{h} \int \omega^n \frac{\partial f(\omega)}{\partial \omega} \mathcal{T}_\sigma(\omega) d\omega, \tag{3}$$

$f(\omega)$ is the Fermi-Dirac distribution function, and $\mathcal{T}_\sigma(\omega)$ is the spin-resolved transmission coefficient. Henceforth we will also use notation $L_n = L_{n\uparrow} + L_{n\downarrow}$ and $M_n = L_{n\uparrow} - L_{n\downarrow}$.

The transport properties can be calculated from Onsager integrals $L_{n\sigma}$ using Eq. (2). In particular, the electrical and spin conductances are

$$G \equiv \partial_V I_C|_{\substack{V_S=0 \\ \Delta T=0}} = e^2 L_0, \tag{4}$$

$$G_S \equiv \partial_{V_S} I_S|_{\substack{V=0 \\ \Delta T=0}} = -e\frac{\hbar}{2} \cdot L_0, \tag{5}$$

correspondingly, where $\partial_x A|_{y=0}$ denotes partial derivative of $A(x, y)$ with respect to x, while the condition $y = 0$ is fulfilled. Similarly, the heat conductance is given by

$$\kappa \equiv \partial_{\Delta T} I_Q|_{\substack{I_C=0 \\ V_S=0}} = \frac{1}{T}\left(L_2 - \frac{L_1^2}{L_0}\right), \tag{6}$$

where the conditions $I_C = 0$ and $V_S = 0$ in fact determine V as a function of ΔT. In this paper we focus on Seebeck and spin Seebeck coefficients, denoted correspondingly by S and S_S,

$$S = G^{-1}\partial_{\Delta T} I_C\Big|_{\substack{V=0 \\ V_S=0}} = -\frac{1}{eT}\frac{L_1}{L_0}, \tag{7}$$

$$S_S = G_S^{-1}\partial_{\Delta T} I_S\Big|_{\substack{V=0 \\ V_S=0}} = -\frac{2}{\hbar T}\frac{M_1}{L_0}. \tag{8}$$

These are related to the (spin) Peltier coefficient $\Pi = \partial_{I_C} I_Q|_{\substack{V_S=0 \\ \Delta T=0}}$ ($\Pi_S = \partial_{I_S} I_Q|_{\substack{V=0 \\ \Delta T=0}}$) by $\Pi_{(S)} = S_{(S)}T$. However, we prefer to study $S_{(S)}$ instead of $\Pi_{(S)}$, because

Seebeck coefficient better captures caloric properties at low temperatures. Finally, we can define the (spin) figure of merit

$$Z_{(S)}T = S^2_{(S)}G_{(S)}T/\kappa, \tag{9}$$

which is a measure of thermodynamic efficiency, and the corresponding power factor

$$Q_{(S)} = S^2_{(S)}G_{(S)}, \tag{10}$$

which is related to maximal power of the device and the performance under the fixed flow conditions [40].

The transmission coefficient is proportional to the imaginary part of the QD1's retarded Green function, $\mathcal{T}_\sigma(\omega) = -\Gamma_\sigma \mathrm{Im}\,\langle\langle d^\dagger_{1\sigma}|d_{1\sigma}\rangle\rangle^{\mathrm{ret}}(\omega)$, which we determine with the aid of the numerical renormalization group (NRG) method [41, 42], building the full density matrix from states discarded during the iteration of the NRG procedure [43, 44]. In calculations we use discretization parameter $\Lambda = 2$ and keep 2048 states at each iteration. To perform the computations, we assume flat densities of leads' states within the cutoff $D = 2U$ and make a transformation to an even-odd basis [45]. This leads us to an effective single-channel formulation of the problem, where for the parallel magnetic configuration the only parameters corresponding to the conduction bands are those related to an effective one, namely Γ, p and $D \equiv 1$.

The NRG method allows us to obtain reliable results in the whole parameter space of the model, in particular, at finite temperatures. However, NRG forces us to limit our considerations to the linear response regime, where a single Fermi level can be defined for both leads and, thus, the logarithmic discretization, being a key ingredient of the procedure, is well defined [41].

III. RELEVANT ENERGY SCALES

The considered device hosts very reach physics at the manifold of energy scales. This can be seen in particular in the temperature dependence of the electrical conductance presented in Fig. 2. For decoupled second dot (*i.e.* for $t = 0$), nonmagnetic leads ($p = 0$) and QD1 energy level in the Coulomb valley ($-U \ll \varepsilon_1 \ll 0$), at temperatures below the Kondo temperature T_K, the conduction band electrons screen the spin of the electron occupying QD1. This screening results in an additional resonance in the local density of states of the first dot at the Fermi level, which gives rise to an enhancement of the conductance G, see the curves for $t = 0$ and $p = 0$ in Figs. 2(a) and (b). In the Kondo regime G can achieve the unitary limit $G = 2e^2/h$, if the dot is tuned to the point of the particle-hole symmetry (PHS), $\varepsilon = -U/2$, as it is done in Fig. 2(a). The maximal conductance outside the PHS point is slightly smaller, see Fig. 2(b). For single quantum dots coupled to ferromagnetic leads, the Kondo temperature can be estimated from scaling approach [46, 47],

$$T_K \approx \sqrt{\frac{\Gamma U}{2}}\,\exp\left[\frac{\pi\varepsilon(\varepsilon+U)}{2\Gamma U}\,\frac{\mathrm{arctanh}(p)}{p}\right]. \tag{11}$$

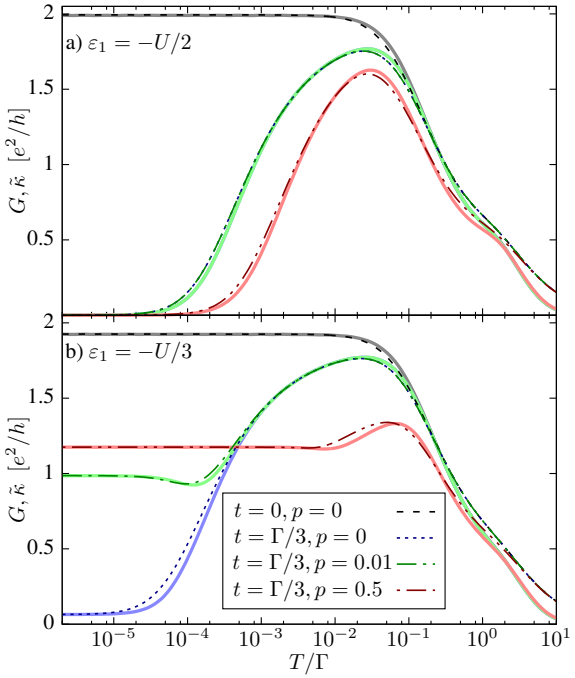

Figure 2. The linear conductance G (dashed lines) as a function of temperature T calculated for $\varepsilon_2 = -U/2$, $\Gamma = U/5$ and (a) $\varepsilon_1 = -U/2$, (b) $\varepsilon_1 = -U/3$. Solid lines indicate the rescaled and shifted thermal conductance, $\tilde{\kappa} \equiv \mathcal{L}_0^{-1}\kappa(\alpha T)/(\alpha T)$ with $\alpha = 2$ (see text for details). In (a) the curves for $p = 0$ and $p = 0.01$ (both for $t = \Gamma/3$) are on top of each other.

Experimentally, the Kondo temperature is typically defined as the temperature at which $G = G_{\max}/2$. For parameters assumed in Fig. 2(a) in the case of $p = 0$ and $t = 0$, from the temperature dependence of G we find $T_K \approx 0.32\Gamma$.

The coupling between quantum dots results in the emergence of another energy scale, T^*, which for relatively weak $t \lesssim \Gamma$ is associated with the screening of second dot's spin by the continuum formed by QD1 and leads. This screening manifests itself through a decrease of G for temperatures below T^*, see the curves for $t = \Gamma/3$, $p = 0$ in Figs. 2(a) and (b). At PHS point the conductance drops to 0 as $G \propto T^2$ [27], while outside this point some finite conductance remains even in the $T = 0$ limit, cf. Fig. 2(b). The temperature at which the second stage of screening takes place can be theoretically estimated from [27, 28]

$$T^* = a\,T_K\,e^{-bT_K/J_{\mathrm{eff}}}, \tag{12}$$

where $J_{\mathrm{eff}} = 4Ut^2/[U^2 - (\varepsilon_1 - \varepsilon_2)^2]$ is the effective exchange interaction between the dots and a, b are numbers of the order of 1. However, similarly to T_K, we estimate T^* numerically from the temperature dependence of G, as the temperature at which the conductance drops to half of its maximum value. For parameters assumed in Fig. 2(a), $p = 0$ and $t = \Gamma/3$, $T^* \approx 5.9 \cdot 10^{-4}\Gamma$.

The influence of leads' ferromagnetism on transport properties differs significantly, depending on the presence or lack of particle-hole symmetry in the system. At PHS point, $\varepsilon_1 = \varepsilon_2 = -U/2$, the leads' spin polarization only slightly modifies T_K and T^*, cf. Eqs. (11) and (12), which also causes some minor change in $G_{\max}$, see Fig. 2(a). However, outside the PHS point this influence is much more pronounced, as can be seen in Fig. 2(b). Even relatively low values of spin polarization (see the curve for $p = 0.01$) block the second stage of Kondo screening, while the value of $p = 0.5$ is sufficient to suppress the Kondo effect completely. This is caused by the fact that, in the case of ferromagnetic leads, the renormalization of double quantum dot energy levels due to the hybridization with electrodes becomes spin-dependent, which implies that an effective exchange field $\Delta\varepsilon_{\rm ex}$ is induced in DQD. $\Delta\varepsilon_{\rm ex}$ strongly depends on the DQD level positions, in particular, $\Delta\varepsilon_{\rm ex} = 0$ at PHS point. For $t \ll \Gamma$, one can reasonably approximate $\Delta\varepsilon_{\rm ex}$ induced in QD1 by the formula for a single quantum dot [47, 48],

$$\Delta\varepsilon_{\rm ex}^{\rm QD1} \approx \frac{2p\Gamma}{\pi} \log\left|\frac{\varepsilon_1}{\varepsilon_1 + U}\right| \tag{13}$$

The determination of the exchange field in the second dot, denoted by $\Delta\varepsilon_{\rm ex}^{\rm QD2}$, is a more subtle problem [34, 48]. Nevertheless, for $t \ll \Gamma$, $\Delta\varepsilon_{\rm ex}^{\rm QD2}$ can be seen as a consequence of coupling between QD2 and the continuum formed by QD1 and the leads. The effective spin-dependent coupling to the second dot $\Gamma_{2\sigma}$ is then proportional to $t^2/\Gamma_\sigma = (1 - \sigma p)\Gamma_2$, with $\Gamma_2 = (\Gamma_{2\uparrow} + \Gamma_{2\downarrow})/2$, instead of simply Γ_σ as in the case of QD1. Note that Γ_2 is a function of both t and p, and the effective spin polarization equals $-p$. Consequently, while the coupling to one of the spin species is larger in the first dot, it can be just opposite in the second dot, which implies that $\Delta\varepsilon_{\rm ex}^{\rm QD1}$ and $\Delta\varepsilon_{\rm ex}^{\rm QD2}$ can have different signs [34]. By raising the exchange field, detuning from the PHS point by changing either ε_1 or ε_2 will generally suppress the second stage of the Kondo effect once $|\Delta\varepsilon_{\rm ex}| \gtrsim T^*$ [35]. Moreover, it can also affect the first-stage Kondo effect if $|\Delta\varepsilon_{\rm ex}| \gtrsim T_K$.

In the strong coupling regime and for $p = 0$, the modified Wiedemann-Franz law was predicted [18, 25, 49], which states that at $T < T_K$, $\mathcal{L} = \kappa(\alpha T)/[\alpha T G(T)]$ is a constant, instead of the Lorentz number $\kappa(T)/[TG(T)]$. The value of this constant equals $\mathcal{L}_0 = (\pi^2/3)\, k_B^2/e^2$, while the scale shift α was estimated to be approximately equal 2. We found the same behavior also in the case of finite spin polarization, although with slightly worse accuracy. This is illustrated in Fig. 2, where rescaled and shifted heat conductance $\tilde{\kappa}(T) \equiv \mathcal{L}_0^{-1}\kappa(2T)/(2T)$ is plotted as a function of T with solid lines. At $T \lesssim T_K$, all curves overlap to good accuracy with $G(T)$, which implies that the modified Wiedemann-Franz law also holds in the case of T-shaped DQDs with ferromagnetic contacts.

IV. THERMOPOWER AND SPIN THERMOPOWER

In this section we present and discuss the results on the Seebeck and spin Seebeck coefficients. First, we study their temperature dependence and then analyze what happens when the degree of leads' spin polarization is varied. Finally, we consider the dependence of thermoelectric coefficients on the position of DQD energy levels.

A. Temperature dependence

The full temperature dependence of (spin) thermoelectric coefficients is presented in Fig. 3 for different values of leads' spin polarization p. We cover there a wide class of ferromagnetic materials, starting with nonmagnetic case and ending with half-metals, for which $p \to 1$. This figure was calculated for $\varepsilon_1 = -U/3$ and $\varepsilon_2 = -U/2$, *i.e.* outside the PHS point, since for $\varepsilon_1 = \varepsilon_2 = -U/2$, the thermopower vanishes due to equal contributions from electron and hole processes. For nonmagnetic systems, the second stage of screening leads to an enhancement of S at very low temperatures of the order of T^* [25]. For finite spin polarization, however, a suppression of the second stage of Kondo effect by the exchange field occurs, cf. Fig. 2, which suppresses the thermopower peak at $T < T^*$, see Fig. 3(a). Clearly, leads' polarization, even as small as $p = 0.01$, is sufficient for the low-temperature peak in $S(T)$ to be strongly suppressed. This is due to the fact that even very low values of p give rise to finite exchange field, cf. Eq. (13), which for $p = 0.01$ can already become larger than T^*. In a similar spirit, larger values of spin polarization resulting in larger exchange field can affect thermopower behavior at higher temperatures. Interestingly, for $T \approx T_K$ one can then observe a more subtle interplay between the Kondo correlations and the exchange field. For $p < 0.5$, $S(T)$ exhibits a dip with $S(T) < 0$ at $T \approx T_K$, which is characteristic of the (single-stage) Kondo effect [18]. On the other hand, with increasing the spin polarization, thermopower changes sign and a positive peak appears instead, see the curves for $p \geq 0.9$ in Fig. 3(a). This can be explained as follows.

For $T^* < T < T_K$ and $p = 0$ there is a Kondo peak visible in the total transmission coefficient $\mathcal{T}(\omega) = \sum_\sigma \mathcal{T}_\sigma(\omega)$, as can be seen in Fig. 4, which presents the energy dependence of $\mathcal{T}(\omega)$ for different spin polarization p. Because $\varepsilon_1 > -U/2$, the Kondo peak displays some asymmetry with respect to the Fermi energy ($\omega = 0$). In fact, finite temperature, which is slightly below T_K, results in a small shift of the maximum to $\omega > 0$. Because of that, $\mathcal{T}(\omega)$ has a finite slope at $\omega = 0$, which is responsible for nonzero thermopower of the device. For $p \neq 0$ the exchange field appears, which grows with increasing p. Thus, for sufficiently large spin polarization, $\Delta\varepsilon_{\rm ex}$ can become larger than T_K. If this is the case the Kondo peak becomes suppressed and split by $2\Delta\varepsilon_{\rm ex}$; see

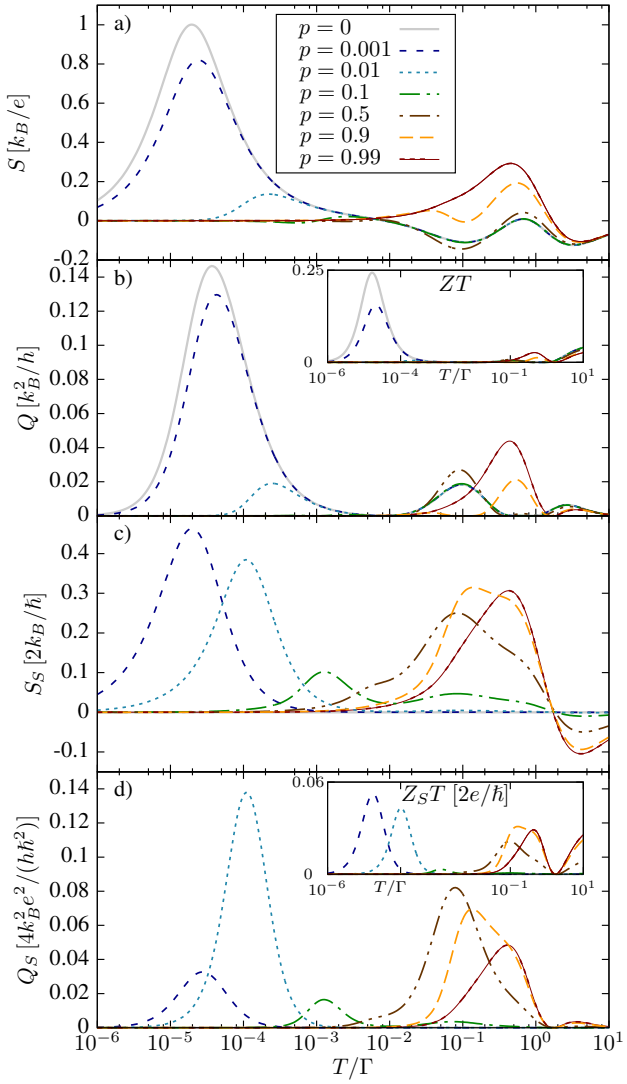

Figure 3. Thermopower (a), the corresponding power factor (b) and the related spin counterparts (c,d) calculated as a function of temperature for $\varepsilon_1 = -U/3$, $\varepsilon_2 = -U/2$, $t = \Gamma/3$ and $\Gamma = U/5$, and for different values of spin polarization p, as indicated. The insets in (b) and (d) show the temperature dependence of the corresponding figures of merit, ZT and Z_ST.

Fig. 4. Moreover, with increasing the spin polarization, the levels of DQD become split and the weight of the transmission coefficient becomes shifted to negative energies. This is visible as a gradual enhancement of the negative-ω Hubbard peak. For very large spin polarization, due to the factors $(1 \pm p)$, the majority spin states are mainly responsible for the enhanced transmission for $\omega < 0$. The above-described behavior results in a sign change of the derivative of $\mathcal{T}(\omega)$ at $\omega = 0$ with increasing p, which gives rise to the associated sign change of the Seebeck coefficient visible in Fig. 3(a).

One could imagine a similar situation for $T \approx T^*$, with a dip in the transmission coefficient corresponding to the second stage of screening being split by $\Delta\varepsilon_{\rm ex}$. However, because $\Delta\varepsilon_{\rm ex}$ becomes larger than T^* already for very small values of spin polarization, e.g. for $p = 0.01$ for parameters assumed in Fig. 3, the difference between $(1-p)$ and $(1+p)$ factors in the spin-resolved transmission coefficient is not significant. For this reason the relative depth of dips remains approximately constant and we do not observe a negative peak at $T \approx T^*$ for any value of spin polarization considered in Fig. 3. However, as presented in Sec. IV B, a sign change of thermopower in the second stage of screening may occur for $p \approx 0.02$ and is even more pronounced for $\varepsilon_1 = -U/4$ instead of $\varepsilon_1 = -U/3$.

The temperature dependence of the power factor corresponding to the Seebeck coefficient shown in Fig. 3(a) is presented in Fig. 3(b). It exhibits local maxima for temperatures corresponding to peaks (or dips) visible in S, including a small peak at $T \approx U$, associated with thermally excited hole-like (due to $\varepsilon_1 < 0$) transport. The inset in Fig. 3(b) displays the thermoelectric figure of merit ZT as a function of temperature. It also exhibits all the peaks of $S(T)$, however, the contributions at intermediate temperatures, $T^* < T < T_K$, are somewhat suppressed by quite large heat conductance; see in particular the curve for $p = 0.01$ in Fig. 3(b).

We now move to the discussion of spin thermoelectric properties of the considered device. A large conventional thermopower present at $T \approx T^*$ gives a hope that breaking the spin-reversal symmetry by finite leads' spin polarization will generate a considerable spin thermopower. However, generation of S_S at such low temperatures is a matter of a delicate compromise. This is because while the spin Seebeck coefficient can be generally enhanced by increasing spin polarization, the second stage of screening and, consequently, the conventional thermopower become strongly suppressed if p is too large, as already explained in the discussion of Fig. 3(a). Nevertheless, as can be inferred from Fig. 3(c), there are such values of spin polarization for which the symmetry is sufficiently broken and a maximum in $S_S(T)$ appears, see

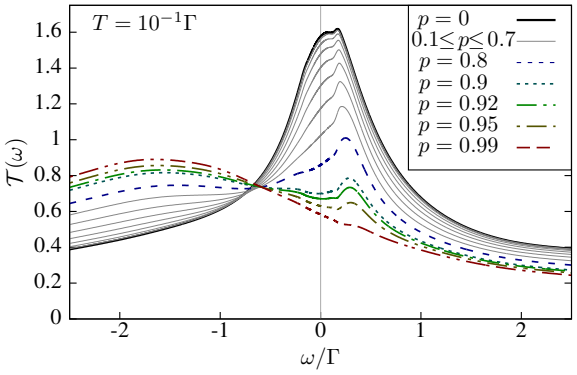

Figure 4. The energy dependence of the total transmission coefficient $\mathcal{T}(\omega) = \sum_\sigma \mathcal{T}_\sigma(\omega)$ calculated for different values of spin polarization p and for parameters corresponding to Fig. 3 with $T = 10^{-1}\Gamma$.

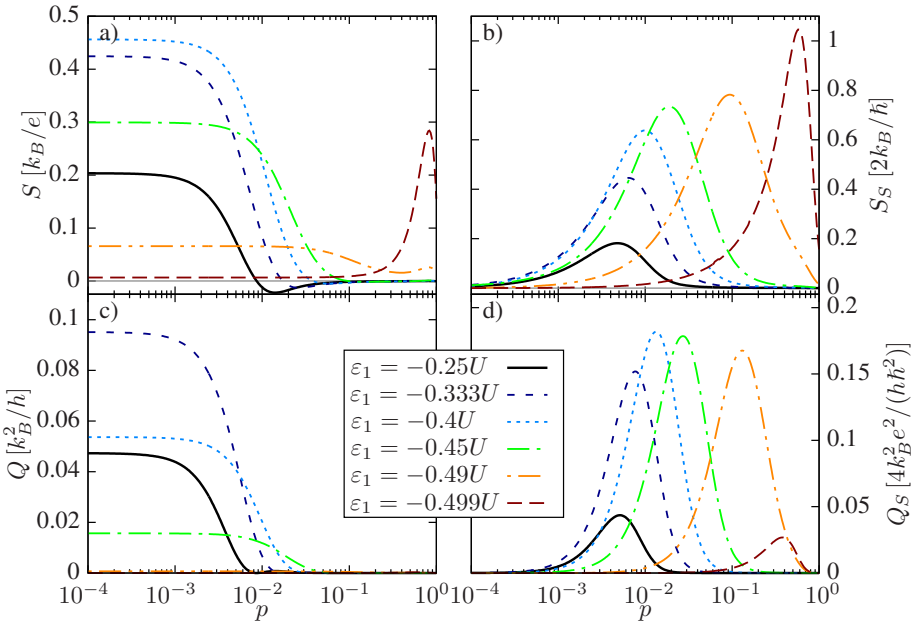

Figure 5. The thermopower (a), spin thermopower (b) and the corresponding power factors, (c) and (d), plotted as a function of spin polarization p for different values of the level position of the first quantum dot, as indicated in the figure. The other parameters are the same as in Fig. 3 with $T = 10^{-4}\Gamma$.

the curves for $p = 0.001$ and $p = 0.01$. We note that $\hbar/2 \cdot S_S^{\max} < eS^{\max}$ for $p = 0.001$ [$S_{(S)}^{\max}$ denotes the maximal value of $S_{(S)}(T)$ for a given value of p], while for $p = 0.01$ the opposite inequality holds. Indeed, in the latter case the spin thermopower exceeds the conventional thermopower.

With increasing the degree of spin polarization of the leads, the maximum in S_S moves to larger temperatures and for $p \geq 0.5$ the spin Seebeck coefficient exhibits a peak at $T \approx T_K$, see Fig. 3(c). Contrary to the case of conventional Seebeck coefficient, the peak at $T \approx T_K$ has the same sign as the low-temperature peak for small spin polarization. This can be surprising, because the peak in $S(T)$ changes sign when T increases from $T \approx T^*$ to $T \approx T_K$, cf. Fig. 3(a). However, in the case of spin Seebeck coefficient one needs to keep in mind that, for assumed parameters, the exchange field in QD1 is opposite to the exchange field in QD2, which compensates for this effect.

One can be surprised that p of the order of one percent is sufficient to induce a significant spin Seebeck coefficient. However, it is advisory to recall, that S_S is in fact a ratio of a small spin bias V_S and a small temperature gradient ΔT. Thus, even the largest value of S_S, despite its fundamental aspects, does not guarantee a practical importance of the result, if the corresponding power factor Q_S is too small. For this reason in Fig. 3(d) we show the temperature dependence of Q_S. It can be clearly seen that the peak in $Q_S(T)$ corresponding to $p = 0.001$ is a few times smaller than the peak corresponding to $p = 0.01$. This remains in agreement with intuition, that the leads' spin polarization with degree much smaller than 1% cannot induce a significant spin current (although this very small spin current can be still much larger then the corresponding charge current). On the other hand, the peaks visible in Q_S for larger temperatures and present for strongly polarized leads are also smaller than the peak in the case of $p = 0.01$. This implies that the thermoelectric performance of the considered device is the best in the regime of the second stage of screening. Nevertheless, the corresponding spin-thermoelectric figure of merit $Z_S T$, which is plotted in the inset of Fig. 3(d), is not too spectacular, with values only slightly exceeding $0.05 \cdot (2e/\hbar)$.

B. Dependence on the leads' spin polarization

In this section we analyze how the spin thermoelectric properties depend on the magnitude of the exchange field, focusing on the second stage of the Kondo effect. We thus assume the same parameters as in the previous section and set $T = 10^{-4}\Gamma$, which is of the order of T^*, and study the dependence on spin polarization for different values of QD1 level position. According to Eq. (13), the exchange field is linear in p and also in ε_1 near the PHS point, since $\log|\varepsilon_1/(\varepsilon_1 + U)| \approx 4(\varepsilon_1 + U/2)/U$. As can be seen in Fig. 5(a), which displays the dependence of S on p, the Seebeck coefficient in the regime of small spin polarization is a nonincreasing function of p (note the logarithmic scale for p in the plot). At sufficiently low spin polarization, S retains its value for a nonmagnetic system. However, for any ε_1 there is some critical value of p, which we denote p_c, above which the Seebeck coefficient becomes suppressed. This critical polarization

decreases monotonically with growing the detuning from the PHS point, and is related to some critical value of the exchange field, $\Delta\varepsilon_{\rm ex}^{\rm c} \approx T^*$, overcoming the second stage of the Kondo effect. As can be seen in Fig. 5(a), the height of $S(p)$ maximum depends on ε_1 in a nonmonotonic manner. This suggest a nontrivial dependence of S on ε_1, which will be explained in the next section.

Moreover, in Fig. 5(a) we can also notice a small sign change of $S(p)$ for $\varepsilon_1 = -U/4$ and $\varepsilon_1 = -U/3$. This is in fact a consequence of the same phenomenon as that responsible for the sign change of $S(T)$ for $T \sim T_K$ described in Sec. IV A. The main difference is that the dip in the transmission coefficient, corresponding to the second stage of the Kondo screening, more easily gets smeared, than split. For this reason, the negative peak of S is rather small and develops only in a narrow range of parameters, see Fig. 5(a).

We also note that very close to the PHS point, one can observe a large peak in $S(p)$, see the curve for $\varepsilon_1 = -0.499U$ in Fig. 5(a). This result, however, may be considered somewhat artificial. According to Eq. (7), S is proportional to the ratio of L_1 and L_0. Exactly at the PHS point, L_1 is always 0 while L_0 decreases with temperature as T^2. Moreover, L_0 is a symmetric function of the detuning from the PHS point, while L_1 is an anti-symmetric function. Thus, for $|\varepsilon_1 - U/2| \gtrsim T$, when L_0 and L_1 are set by detuning, S may reach really large values. The role of spin polarization is here to split the transmission coefficient dip and cause $\mathcal{T}(\omega)$ to possess a finite slope at $\omega = 0$, which additionally enhances L_1. However, despite large value of S, the system does not conduct in this regime (neither heat, nor current, nor spin), so the result is not really physically interesting. This is confirmed by the values of Q, which is presented in Fig. 5(c). While for $\varepsilon_1 > -0.49U$, the peaks of $S(p)$ correspond to the peaks of $Q(p)$, this is not the case for $\varepsilon_1 = -0.499U$; Q is not enhanced in the regime of large p.

The dependence of the spin Seebeck coefficient S_S on p is presented in Fig. 5(b). It significantly differs from the p-dependence of S, since S_S vanishes for $p = 0$. In fact, $S_S(p)$ exhibits a peak, whose position varies with ε_1 by a few orders of magnitude. The height of the peak increases when ε_1 approaches the PHS point. The existence of this peak is a consequence of a balance between the exchange field and the second stage of screening. If p is small enough, spin-reversal symmetry is approximately preserved and $S_S \approx 0$. On the other hand, large values of spin polarization result in strong exchange field, which destroys the second stage of the Kondo effect, and thus decrease the spin caloritronic effects.

The exchange field can be also changed by tuning ε_1, which allows for moving the peak in $S_S(p)$ to the desired range of p. The flexibility of the device upon this kind of tuning is reduced by the power factor corresponding to spin thermoelectric effects, Q_S, which is shown in Fig. 5(d). Q_S as a function of p exhibits peaks corresponding to those present in $S_S(p)$ for all values of

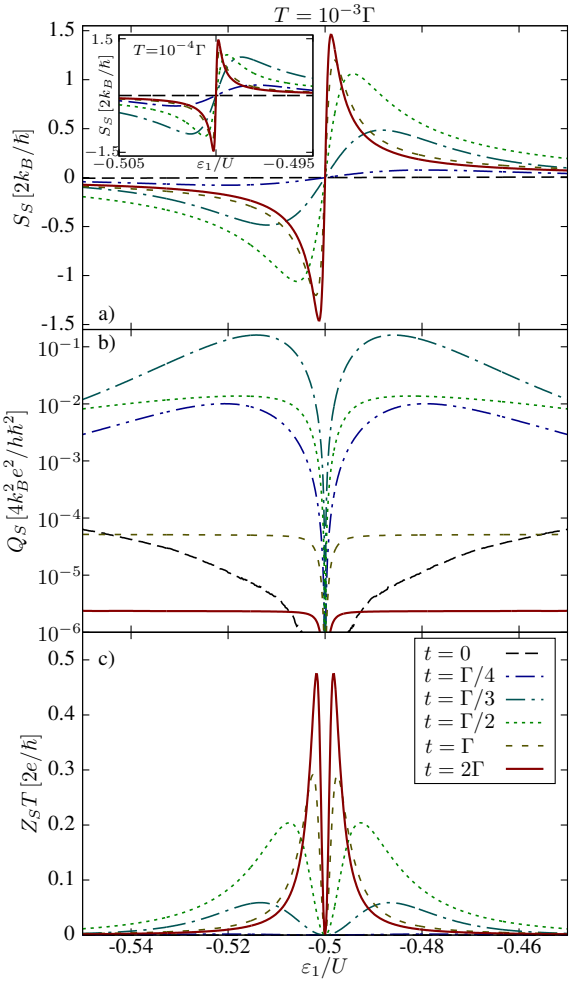

Figure 6. The spin thermopower (a), the corresponding power factor (b) and the spin-thermoelectric figure of merit Z_ST (c) as a function of ε_1 calculated for different values of hopping between the two dots, as indicated. The parameters are the same as in Fig. 3 with $T = 10^{-3}\Gamma$ and $p = 0.5$. The inset shows peaks of the spin thermopower at lower $T = 10^{-4}\Gamma$.

ε_1 considered. The height of these peaks is the largest for $-0.49U < \varepsilon_1 < -U/3$ and drops significantly for $|\varepsilon_1 + U/2| < 0.01$. This is associated with the suppression of the conductance already discussed in the case of conventional Seebeck coefficient. Moreover, as can be seen in Fig. 5, for a finite value of spin polarization, there exists such a value of ε_1 for which large peaks in $S_S(p)$ and $Q_S(p)$ occur.

C. Dependence on the position of QD1 energy level

As follows from Fig. 5, the dependence of S_S on ε_1 for large p is quite sharp. This is related to Fano-like interference, which occurs between transport paths through a weakly coupled molecular state of DQD that is a resonant one and another, strongly coupled state serving as the background [28, 29, 31, 32]. To shed more light on this

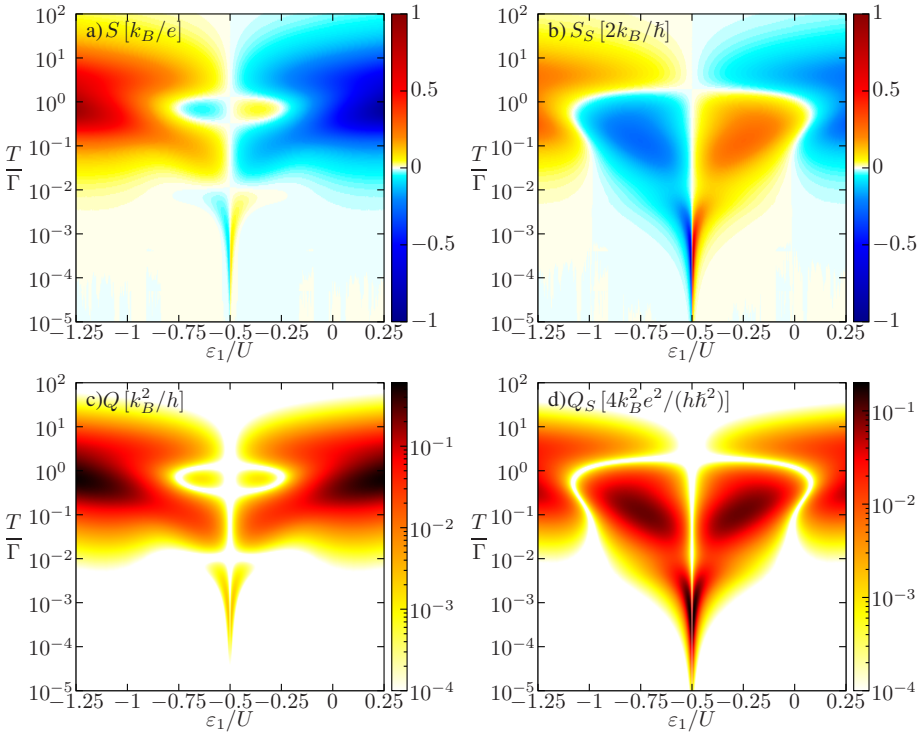

Figure 7. The dependence of thermopower (a), spin thermopower (b) and the corresponding power factors, (c) and (d), on the first dot level position ε_1 and temperature T. The parameters are the same as in Fig. 3 with $p = 0.5$. Note the logarithmic color scale for the power factors.

behavior, in Fig. 6 we now plot the full ε_1-dependence of S_S for fixed $p = 0.5$ and the other parameters the same as in Fig. 5. In this figure we also study the influence of different hopping between the dots t, which strongly affects the formation of molecular states in DQD and, thus, strongly influences the interference effects.

The dependence of S_S on ε_1 calculated at $T = 10^{-4}\Gamma$, *i.e.* for temperature corresponding to that used in Fig. 5, is shown as an inset to Fig. 6(a). However, in this case for the considered range of ε_1 the spin-thermoelectric power factor Q_S is quite small, as explained in the previous section (not shown in the plot). Moreover, it becomes even more suppressed with increasing t. For this reason, the main results shown in Fig. 6 are calculated at larger temperature, $T = 10^{-3}\Gamma$, which is of the order of T^* for $t = \Gamma/3$. At this temperature, outside the PHS point, the conductance is not yet fully suppressed due to the second stage of Kondo effect, and Q_S values are larger, as can be seen in Fig. 6(b).

At first sight, one can immediately notice a striking qualitative similarity between the curves shown in Fig. 6(a) and those in the inset. A closer look, however, reveals some differences. First of all, the two plots have different scales for the horizontal axis. It turns out that the sharp interference peaks get broadened with increasing the temperature. Moreover, the width of those peaks scales approximately linearly with T, while the maximal value of S_S is rather independent of temperature. We also note that S_S is anti-symmetric around the PHS point, which is caused by the corresponding sign change of the exchange field $\Delta\varepsilon_{\rm ex}$ around this point.

The spin-thermoelectric power factor as a function of ε_1 is shown in Fig. 6(b). One can clearly see that Q_S is optimized for $t = \Gamma/3$ and only in this case reaches considerable values. For smaller values of hopping t, the temperature considered in Fig. 6(b) is above T^* and S_S is not enhanced. On the other hand, for larger hoppings, $T \ll T^*$ and the conductance is generally blocked by the second stage of screening. Since Q_S must be sufficiently large for any measurement to be possible, one should not overestimate the meaning of large spin-thermoelectric figure of merit. With this in mind, let us analyze Fig. 6(c), which presents Z_ST as a function of ε_1.

As can be seen in the figure, Z_ST exhibits maxima for such values of ε_1 for which $|S_S|$ has peaks. Due to the square dependence of Z_ST on S_S, cf. Eq. (9), the differences in peaks' heights are now more prominent than in the case of S_S. The influence of thermal and electrical conductances compensates each other. The maximal Z_ST equals $0.5 \cdot 2e/\hbar$, which is quite large, see Fig. 6(c). However, it occurs for strong t, for which Q_S is rather low and the measurement is hardly possible. On the other hand, for $t = \Gamma/3$, corresponding to reasonably large Q_S, maximal Z_ST remains of the order of $0.1 \cdot 2e/\hbar$.

Finally, to make the analysis of (spin) thermoelectric properties of our magnetic device complete, in Fig. 7 we

present the thermopowers and the corresponding power factors as a function of temperature and QD1 energy level. One can see that both S and S_S change sign in the PHS point. However, S as a function of T exhibits more sign changes than $S_S(T)$. The regimes of large Seebeck and spin Seebeck coefficients can be clearly identified in the figure. While for S and Q the largest values are obtained at relatively high T and large detunings from the PHS point, S_S and Q_S are maximized for temperatures of the order of T^* and close to (but not at) the PHS point.

V. CONCLUSIONS

We have analyzed the thermoelectric and spin-thermoelectric properties of the double quantum dot in a T-shaped configuration, coupled to two leads magnetized in parallel. The calculations were performed in the linear response regime with the aid of the NRG and we focused on the parameter regime where the system exhibits the two-stage Kondo effect. We determined the full temperature dependence of the (spin) Seebeck coefficient, together with the corresponding power factor and figure of merit. We also studied the dependence of the spin caloritronic properties on the degree of spin polarization of the leads, dot level detuning and the strength of hopping between the dots. It was demonstrated that the thermal conductance fulfills the modified Wiedemann-Franz law found previously for nonmagnetic systems. In addition, we showed that the spin Seebeck coefficient can be strongly enhanced in the regime corresponding to the second stage of the Kondo effect. This enhancement is very sensitive to the value of leads' spin polarization. Moreover, it can be tuned by changing the DQD parameters, such as level position and hopping between the dots. We also showed that in order to keep the power factor at an experimentally relevant level, one needs to set the temperature of the order of T^*. Since T^* strongly depends on t, this effect can be tuned by changing the hopping between the dots and the temperature.

We would also like to emphasize that the spin thermoelectric properties of the considered device are very sensitive to the spin polarization of the leads, and even small values of p (of the order of 1%) can induce large spin Seebeck effect. Such a value of spin polarization may be a consequence of current-induced spin accumulation even for very small driving currents. It can also occur in the case of the anti-parallel configuration of leads' magnetizations for two asymmetrically coupled electrodes. Then, even very small coupling asymmetry changes the effective spin polarization from 0 to a finite value of $p = (\Gamma_L - \Gamma_R)/\Gamma$. It therefore seems quite realistic to expect $p \gtrsim 0.01$ in an experiment, which will cause the conventional Seebeck effect to be strongly suppressed (compared to nonmagnetic case) and the spin Seebeck effect to be present and even possibly strong. All these implies that the effects studied in this paper may be also relevant for a system, in which one would not expect them to appear.

ACKNOWLEDGMENTS

This work was supported by the National Science Centre in Poland through Grant No. DEC-2012/04/A/ST3/00372.

[1] R. D. Barnard, *Thermoelectricity in Metals and Alloys* (Taylor&Francis, London, 1972).

[2] L. D. Hicks, M. S. Dresselhaus, *Effect of quantum-well structures on the thermoelectric figure of merit*, Phys. Rev. B **47**, 12727 (1993).

[3] L. D. Hicks, M. S. Dresselhaus, *Thermoelectric figure of merit of a one-dimensional conductor*, Phys. Rev. B **47**, 16631 (1993).

[4] M. Krawiec and K. I. Wysokiński, *Thermoelectric effects in strongly interacting quantum dot coupled to ferromagnetic leads*, Phys. Rev. B **73**, 075307 (2006).

[5] R. Świrkowicz, M. Wierzbicki, and J. Barnaś, *Thermoelectric effects in transport through quantum dots attached to ferromagnetic leads with noncollinear magnetic moments*, Phys. Rev. B **80**, 195409 (2009).

[6] M. Esposito, K. Lindenberg and C. Van den Broeck, *Thermoelectric efficiency at maximum power in a quantum dot*, Europhys. Lett. **85**, 60010 (2009).

[7] David M.-T. Kuo and Yia-chung Chang, *Thermoelectric and thermal rectification properties of quantum dot junctions*, Phys. Rev. B **81**, 205321 (2010).

[8] Jie Liu, Qing-feng Sun, and X. C. Xie, *Enhancement of the thermoelectric figure of merit in a quantum dot due to the Coulomb blockade effect*, Phys. Rev. B **81**, 245323 (2010).

[9] M. Tsaousidou and G. P. Triberis, *Thermoelectric properties of a weakly coupled quantum dot: enhanced thermoelectric efficiency*, J. Phys.: Condens. Matter **22**, 355304 (2010).

[10] Yu-Shen Liu, Feng Chi, Xi-Feng Yang and Jin-Fu Feng, *Pure spin thermoelectric generator based on a rashba quantum dot molecule*, J. Appl. Phys. **109**, 053712 (2011).

[11] Bhaskaran Muralidharan and Milena Grifoni, *Performance analysis of an interacting quantum dot thermoelectric setup*, Phys. Rev. B **85**, 155423 (2012).

[12] Rafael Sanchez, Björn Sothmann, Andrew N Jordan and Markus Büttiker, *Correlations of heat and charge currents in quantum-dot thermoelectric engines*, New J. Phys. **15**, 125001 (2013).

[13] Ł. Karwacki, P. Trocha and J. Barnaś, *Spin-dependent thermoelectric properties of a Kondo-correlated quantum dot with Rashba spin-orbit coupling*, J. Phys.: Condens.

Matter **25**, 505305 (2013).
[14] Sun-Yong Hwang, Rosa Lopez, David Sanchez, *Large thermoelectric power and figure of merit in a ferromagnetic-quantum dot-superconducting device*, arXiv:1512.06242v1 (unpublished).
[15] J. Kondo, *Resistance Minimum in Dilute Magnetic Alloys*, Prog. Theor. Phys. **32**, 37 (1964).
[16] D. Goldhaber-Gordon, H. Shtrikman, D. Mahalu, D. Abusch-Magder, U. Meirav, M. A. Kastner, *Kondo effect in a single-electron transistor*, Nature (London) **391**, 156 (1998).
[17] S. Cronenwett, T. H. Oosterkamp, L. P. Kouwenhoven, *A tunable Kondo effect in quantum dots*, Science **281**, 182 (1998).
[18] T. A. Costi and V. Zlatić, *Thermoelectric transport through strongly correlated quantum dots*, Phys. Rev. B **81**, 235127 (2010).
[19] R. Scheibner, H. Buhmann, D. Reuter, M. N. Kiselev, and L. W. Molenkamp, *Thermopower of a Kondo Spin-Correlated Quantum Dot*, Phys. Rev. Lett. **95**, 176602 (2005).
[20] S. Donsa, S. Andergassen, and K. Held, *Double quantum dot as a minimal thermoelectric generator*, Phys. Rev. B **89**, 125103 (2014).
[21] T. Rejec, R. Zitko, J. Mravlje, and A. Ramsak, *Spin thermopower in interacting quantum dots*, Phys. Rev. B **85**, 085117 (2012).
[22] I. Weymann, J. Barnaś, *Spin thermoelectric effects in Kondo quantum dots coupled to ferromagnetic leads*, Phys. Rev. B **88**, 085313 (2013).
[23] I. Weymann, *Boosting spin-caloritronic effects by attractive correlations in molecular junctions*, Sci. Rep. **6**, 19236 (2016).
[24] P. Trocha and J. Barnaś, *Large enhancement of thermoelectric effects in a double quantum dot system due to interference and Coulomb correlation phenomena*, Phys. Rev. B **85**, 085408 (2012).
[25] K.P. Wójcik, I. Weymann, *Thermopower of strongly correlated T-shaped double quantum dots*, Phys. Rev. B **93**, 085428 (2016).
[26] M. Pustilnik and L. I. Glazman, *Kondo Effect in Real Quantum Dots*, Phys. Rev. Lett. **87**, 216601 (2001).
[27] P. S. Cornaglia and D. R. Grempel, *Strongly correlated regimes in a double quantum dot device*, Phys. Rev. B **71**, 075305 (2005).
[28] R. Žitko and J. Bonča, *Enhanced conductance through side-coupled double quantum dots*, Phys. Rev. B **73**, 035332 (2006).
[29] P. Trocha and J. Barnaś, *Quantum interference and Coulomb correlation effects in spin-polarized transport through two coupled quantum dots*, Phys. Rev. B **76**, 165432 (2007).
[30] R. Žitko, *Fano-Kondo effect in side-coupled double quantum dots at finite temperatures and the importance of two-stage Kondo screening*, Phys. Rev. B **81**, 115316 (2010).
[31] U. Fano, *Effects of Configuration Interaction on Intensities and Phase Shifts*, Phys. Rev. **124**, 1866 (1961).
[32] S. Sasaki, H. Tamura, T. Akazaki, and T. Fujisawa, *Fano-Kondo Interplay in a Side-Coupled Double Quantum Dot*, Phys. Rev. Lett. **103**, 266806 (2009).
[33] L. G. G. V. Dias da Silva, E. Vernek, K. Ingersent, N. Sandler, and S. E. Ulloa, *Spin-polarized conductance in double quantum dots: Interplay of Kondo, Zeeman, and interference effects*, Phys. Rev. B **87**, 205313 (2013).
[34] K.P. Wójcik, I. Weymann, *Perfect spin polarization in T-shaped double quantum dots due to the spin-dependent Fano effect*, Phys. Rev. B **90**, 115308 (2014).
[35] K.P. Wójcik, I. Weymann, *Two-stage Kondo effect in T-shaped double quantum dots with ferromagnetic leads*, Phys. Rev. B **91**, 134422 (2015).
[36] K. Uchida, S. Takahashi, K. Harii, J. Ieda, W. Koshibae, K. Ando, S. Maekawa, and E. Saitoh, *Observation of the spin Seebeck effect*, Nature **455**, 778 (2008).
[37] J. Flipse, F. L. Bakker, A. Slachter, F. K. Dejene, and B. J. van Wees, *Direct observation of the spin-dependent Peltier effect*, Nature Nanotechnology **7**, 166 (2012).
[38] P. W. Anderson, *Localized Magnetic States in Metals*, Phys. Rev. **124**, 41 (1961).
[39] K.P. Wójcik, I. Weymann, J. Barnaś, *Asymmetry-induced effects in Kondo quantum dots coupled to ferromagnetic leads*, J. Phys.: Condens. Matt. **25**, 075301 (2013).
[40] D. Narducci, *Do we really need high thermoelectric figures of merit? A critical appraisal to the power conversion efficiency of thermoelectric materials*, App. Phys. Lett. **99**, 102104 (2011).
[41] K.G. Wilson, *The renormalization group: Critical phenomena and the Kondo problem*, Rev. Mod. Phys. **47**, 773 (1975).
[42] We use (modified) open-access Budapest Flexible DM-NRG code, http://www.phy.bme.hu/dmnrg/; O. Legeza, C. P. Moca, A. I. Tóth, I. Weymann, G. Zaránd, *Manual for the Flexible DM-NRG code*, arXiv:0809.3143 (unpublished).
[43] F.B. Anders, A. Schiller, *Real-Time Dynamics in Quantum-Impurity Systems: A Time-Dependent Numerical Renormalization-Group Approach*, Phys. Rev. Lett. **95**, 196801 (2005); *Spin precession and real-time dynamics in the Kondo model: Time-dependent numerical renormalization-group study*, Phys. Rev. B **74**, 245113 (2006).
[44] A. Weichselbaum, J. von Delft, *Sum-Rule Conserving Spectral Functions from the Numerical Renormalization Group*, Phys. Rev. Lett. **99**, 076402 (2007).
[45] L. I. Glazman, M. E. Raikh, *Resonant Kondo transparency of a barrier with quasilocal impurity states*, J. Exp. Theor. Phys. Lett. **47**, 452 (1988); Pis'ma Zh. Exp. Teor. Fiz. **47**, 378 (1988).
[46] F. D. M. Haldane, *Scaling Theory of the Asymmetric Anderson Model*, Phys. Rev. Lett. **40**, 416 (1978).
[47] J. Martinek, Y. Utsumi, H. Imamura, J. Barnaś, S. Maekawa, J. König, and G. Schön, *Kondo Effect in Quantum Dots Coupled to Ferromagnetic Leads*, Phys. Rev. Lett. **91**, 127203 (2003).
[48] K. P. Wójcik, *Ferromagnets-induced splitting of molecular states of T-shaped double quantum dots*, Eur. Phys. J. B **88**, 110 (2015).
[49] R. Franz, G. Wiedemann, *Ueber die Wärme-Leitungsfähigkeit der Metalle*, Annalen der Physik **165**, 497 (1853).